Raman Studies of Semiconducting Oxide Nanobelts

K. Mcguire,[a] Z. W. Pan,[b] Z. L. Wang,[b] D. Milkie,[c]
J. Menéndez,[c] and A. M. Rao[a,*]

[a] *Department of Physics and Astronomy, Clemson University, Clemson, South Carolina, USA*
[b] *Center for Nanoscience and Nanotechnology, School of Materials Science and Engineering,
Georgia Institute of Technology, Atlanta, Georgia, USA*
[c] *Department of Physics and Astronomy, Arizona State University, Tempe, Arizona, USA*

Crystalline nanobelts of ZnO and SnO$_2$ were prepared from a thermal evaporation of oxide powders inside an alumina tube in the absence of catalysts. Typical dimensions of the nanobelt samples ranged from ∼10 to 100 μm in length, 30 to 300 nm in width, and 6 to 30 nm in thickness. Room temperature Raman spectra were obtained on pressed mats of nanobelt samples and compared with the corresponding spectra of the starting oxide powders and bulk materials. Collectively, our Raman data indicated that the as-prepared nanobelt samples used in this study were oxygen deficient. Upon annealing at 900 °C in flowing oxygen for 1 h, the nanobelt samples exhibited Raman features that corresponded to those expected in respective bulk semiconducting oxides. The dimensions of the nanobelts were a bit too large to expect significant quantum size effects on the phonon structure similar to those observed in carbon nanotubes and short-period semiconductor superlattices.

Keywords: Nanobelts, ZnO, SnO$_2$, Raman Spectroscopy.

1. INTRODUCTION

Continued interest in the synthesis and properties of nanoscale materials such as nanotubes and nanowires has led to the recent discovery of semiconducting oxide nanobelts.[1] Ultralong belt-like nanostructures of zinc, tin, indium, cadmium, and gallium semiconducting oxides were recently prepared by evaporation of commercial metal oxides at high temperatures.[1] Bulk crystalline SnO$_2$ and SnO$_2$ nanoparticles are currently being used as transparent electrodes[2] and in gas-sensing applications.[3] ZnO films and nanoparticles have found many applications, such as transparent conductive films, solar cell windows, and photocatalysis, as well as being a potential candidate for photonic devices in the ultraviolet range.[4] These semiconducting oxides in nanostructured forms offer new areas of fundamental research and applications. For example, ultraviolet lasing in ZnO nanowire arrays in which the nanowire diameters range between 20 and 150 nm has been recently demonstrated.[5] In this paper, we focus on the Raman scattering properties of SnO$_2$ and ZnO nanobelts with typical widths of 30–300 nm, width-to-thickness ratios of 5–10, and lengths of up to a few millimeters. The width dimension of the nanobelts is in the regime where the quantum confinement phenomenon may occur.

2. EXPERIMENTAL DETAILS

2.1. Synthesis

A detailed description of SnO$_2$ and ZnO nanobelt synthesis can be found in Ref. 1. Briefly, nanobelt synthesis is based on the thermal evaporation of oxide powders in an alumina tube under controlled conditions without catalyst material.[1] The typical evaporation time was ∼2 h, the alumina tube pressure was ∼300 torr, and the argon flow rate was ∼50 sccm. The nanobelts were deposited at the end of the tube on aluminum substrates. XRD confirmed that the SnO$_2$ nanobelts have a rutile structure, the same as bulk crystalline SnO$_2$, with lattice constants of $a = 4.722$ Å and $c = 3.184$ Å.[1] A similar analysis was performed on the ZnO nanobelts, which were identified to have a wurtzite structure (like that in bulk ZnO) with lattice constants $a = 3.249$ Å and $c = 5.206$ Å. Moreover, high-resolution transmission electron microscopy confirmed that the nanobelts were crystalline and dislocation free.[1]

2.2. Raman Spectroscopy

Room-temperature Raman spectra were collected from pressed mats of SnO$_2$ and ZnO nanobelt samples with excitation wavelengths from a Spectra Physics Stabilite 2017 argon ion laser (488 and 514.5 nm) and a Spectra Physics 2080 Krypton ion laser (647.1 nm). With a series of lenses, the beam was focused to a 0.1 mm × 3 mm

---

strip image on the sample. All Raman data were collected in a back-scattering geometry with a Kaiser Optics holographic notch filter employed for the rejection of Rayleigh scattered light from the sample. A SPEX Triax 550 single-grating spectrometer with a liquid nitrogen-cooled CCD detector was used for the collection of the Raman spectra.

3. RESULTS AND DISCUSSION

The Raman spectra for the SnO_2 nanobelts with the 488-, 514.5-, and 647.1-nm excitation wavelengths are shown in the top panel of Figure 1. For comparison, Raman spectra were also obtained from the starting powder materials used in the nanobelt synthesis. For all three excitation wavelengths, two peaks at ~ 112 cm^{-1} and ~ 210 cm^{-1} were observed in the Raman spectra for the starting powders, confirming its stoichiometric composition as SnO. As an example, the bottom panel of Figure 1 shows the spectrum of the starting powders excited with 488 nm. All other features are broad and/or at least one order of magnitude weaker compared with the 112 cm^{-1} and 210 cm^{-1} peaks, suggesting that the two strong Raman peaks correspond to SnO, not SnO_2. In bulk SnO_2, four Raman active modes are expected at 123 cm^{-1} (B_{1g}), 476 cm^{-1} (E_g), 634 cm^{-1} (A_{1g}), and 778 cm^{-1} (B_{2g}).[6–8] The B_{1g} phonon corresponds to a librational motion of octahedra.[6] It was first detected by Peercy and Morosin[7] in single crystalline SnO_2, but its Raman intensity is so weak that it is not commonly observed. There is no discernible B_{1g} peak in any of the spectra in Figure 1. With magnification of the spectra in Figure 1 by 20×, peaks visible at 476 cm^{-1} and 627 cm^{-1} can be assigned to the E_g and A_{1g} peaks expected for SnO_2. Upon further magnification (200×), a weak shoulder is observed in the vicinity of 776 cm^{-1}, which could be assigned to the B_{2g} mode in SnO_2 (not shown in Fig. 1). Furthermore, Raman

peaks corresponding to SnO are weakly present in the nanobelt spectra in Figure 1.

The two dominant peaks seen in the nanobelt spectra in Figure 1 are present at ~ 145 cm^{-1} and ~ 171 cm^{-1}. Sangaletti et al.[9] have carried out Raman studies involving oxidation of Sn films on alumina substrates that were systematically heat-treated in air for 5 h from 250 °C to 650 °C in intervals of 100 °C. After each annealing step, Raman and X-ray diffraction data were obtained to correlate Raman spectral changes with corresponding stoichiometric composition of their films. Two new Raman peaks appeared at 145 cm^{-1} and 171 cm^{-1} and were identified with a stoichiometric SnO_x phase ($1 < x < 2$).[9] Known phases with this intermediate degree of oxidation are Sn_2O_3 and Sn_3O_4.[10, 11] In a similar but independent study, Geurts et al.[12] annealed SnO films grown on glass substrates under 760-Torr oxygen for 10 min over the same temperature intervals as Sangaletti et al.[9] Geurts et al.[12] found dominant peaks at 126 cm^{-1} and 171 cm^{-1}. The first peak agrees with the high-energy Raman peak in metallic β-Sn.[13] This is consistent with the X-ray data, which confirms the presence of β-Sn in the partially oxidized samples. Combined, these results indicate that the 145 cm^{-1} and the 171 cm^{-1} peaks do not correspond to the same stoichiometric phase. Hence we conclude that Sangaletti's samples and our nanobelt samples contain at least two partially oxidized stoichiometric phases, which could be Sn_2O_3/Sn_3O_4 or some other unknown phase.

We next focus our discussion on the origin of weak peaks in the 20× spectra in Figure 1. For clarity, in Figure 2, we reproduce the spectrum of a SnO_2 sample collected with 488-nm excitation along with a phonon density of states (DOS) calculation by K. Parlinski, using PHONON software.[14] This author recently published the first *ab initio* calculation of phonons in SnO_2,[14] and his calculated frequencies are in excellent agreement with the known IR and Raman spectra of SnO_2. In the presence
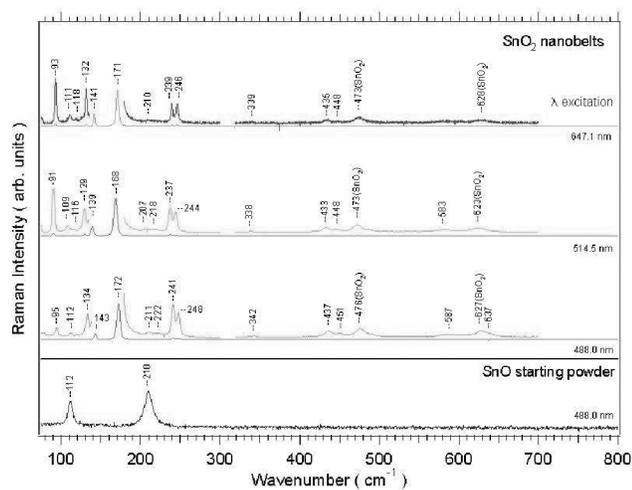

Fig. 1. Raman spectra collected from as-prepared SnO_2 nanobelt (top) and starting powder (bottom) samples. The label $\lambda_{excitation}$ refers to the laser excitation wavelength. All magnified spectra are 20×.
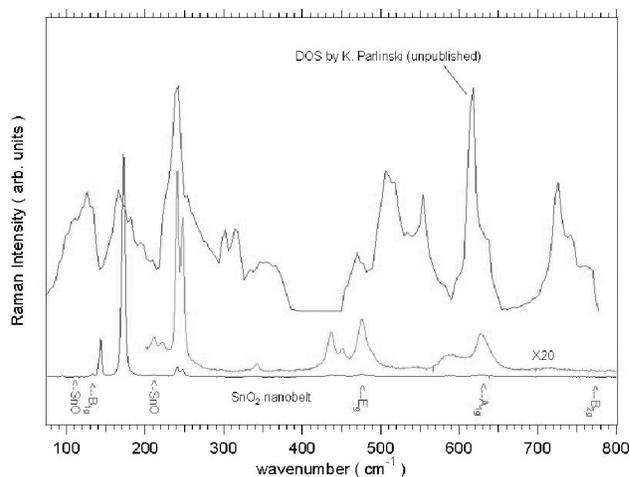
**Fig. 2.** Comparison of a 488-nm SnO_2 nanobelt spectrum with the calculated density of states (see text).

of structural defects, selection rules for off-zone centered Raman modes are relaxed, and one might expect additional Raman peaks at frequencies that coincide with sharp features in the phonon DOS. Indeed, we find some intriguing correlations between the calculated DOS and our Raman spectra. For example, the experimental peaks at $\sim$240 cm^{-1} and $\sim$717 cm^{-1} agree well with peaks in the DOS. Similarly, the strongest peak observed at $\sim$170 cm^{-1} matches a relatively broader peak in the DOS spectrum. Because of the narrower line width for the $\sim$170 cm^{-1} peak, its origin is not assigned to defect-induced scattering. Moreover, if the $\sim$170 cm^{-1} peak was due to defect-induced Raman scattering in SnO_2 (rather than to standard first-order Raman scattering from an intermediately oxidized stoichiometric phase, as we concluded above), an inspection of the DOS suggests that this peak should not dominate the Raman spectrum. An alternative way to explain the $\sim$170 cm^{-1} peak in terms of SnO_2 (and simultaneously explain its narrow width) would be to assume a periodicity increase in some special direction. An inspection of the phonon dispersion curves calculated by Parlinski confirms that there is a 170 cm^{-1} phonon at the R point of the Brillouin zone. This point is folded back to the zone-center phonon if the periodicity is doubled along the (011) direction. However, such periodicity doubling fails to explain the strong 142 cm^{-1} Raman peak. This line does agree with a zone edge phonon in Parlinski's calculation, but this time along the (001) direction. We thus find no obvious way to increase the periodicity and explain all extra Raman peaks, confirming that the most likely explanation for the 142 cm^{-1} and 171 cm^{-1} peaks is the presence of stoichiometric phases with intermediate oxidation. It should be mentioned that our subsequent studies[15] on SnO_2 nanobelts found a wide range of oxygen content in the samples.

In experiments on SnO_2 nanoparticles, a strong broad peak is reported near 580 cm^{-1} to the low-energy side of the *bulk* SnO_2 A_{1g} mode at 634 cm^{-1}.[16–18] The ratio of the two peaks was strongly correlated with the size of the nanoparticles.[16–18] A weak peak at $\sim$580 cm^{-1} is observed in our SnO_2 samples. The ratio of intensities with respect to the 626 cm^{-1} mode in our nanobelt sample is on the order of 1/3, which in the case of nanoparticles corresponds to a surface/volume ratio of 0.075 nm^{-1}. For the nanobelts the same surface/volume ratio would correspond to a nanobelt width of $\sim$30 nm, which is somewhat lower, but not too different from the experimentally determined widths in the 50–200-nm range.[1] The most striking aspect of the 580 cm^{-1} peak in our sample is its narrow width. This, however, may be understandable if we also assign this peak to a surface mode.

Figure 3 illustrates the spectra of ZnO nanobelts (top panel) collected at three different excitation wavelengths. The Raman spectrum of the starting ZnO powder excited with 488 nm is depicted in the bottom panel of Figure 3. As can be seen in the figure, the nanobelt spectra differ
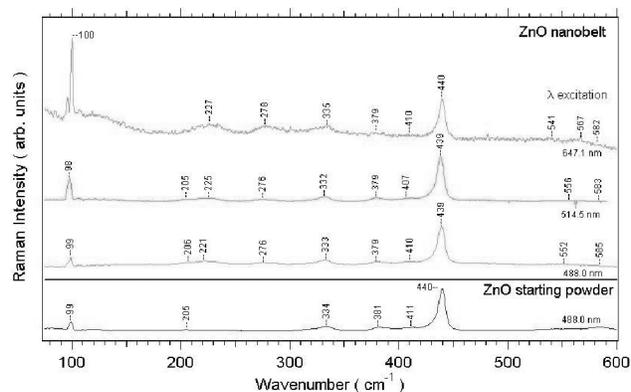
Fig. 3. Top: Raman spectra of as-prepared ZnO nanobelts. Bottom: Raman spectrum of starting ZnO powder sample (see text).

very little from the corresponding spectra for the powder sample. Peaks at 101 cm^{-1} (E_2), 380 cm^{-1} (A_1(TO)), 407 cm^{-1} (E_1(TO)), 437 cm^{-1} (E_2), and 583 cm^{-1} (E_1(LO))[20, 21] are expected for bulk ZnO. These modes can be accounted for in the powder as well as the nanobelt sample, with the exception of the 583 cm^{-1} mode being absent in the nanobelt spectra. The peaks that appear at 205 cm^{-1}, 334 cm^{-1}, and above 800 cm^{-1} have been assigned as second order modes.[20–22] The noteworthy differences that occur between the spectra of the ZnO powder and the nanobelts are the appearance of the modes at 221 cm^{-1}, 276 cm^{-1}, and 553 cm^{-1} and the absence of the 585 cm^{-1} (E_1(LO)) mode. B_2 silent modes between 250 and 300 cm^{-1} in phonon dispersion curves of single crystalline ZnO were reported previously.[23] The peak at 276 cm^{-1} could be attributed to activation of the silent B_2 mode. Tzolov et al. reported a peak at this same position and assumed it to be from the electric field-induced Raman activity of this silent B_2 mode.[20] The appearance of the mode at 221 cm^{-1} has also been reported by other groups working with ZnO films. Xu et al. noticed the appearance of this peak in their Raman spectrum of ZnO films and found that it disappeared with increasing substrate temperature.[24] This 221 cm^{-1} peak was attributed to oxygen vacancies within the films.[24] Furthermore, a peak at 556 cm^{-1}, which is associated with oxygen deficiency in the sample, was also reported by Xu et al.

Since Raman spectroscopic data consistently suggested oxygen-deficient phases in the nanobelt samples used in this study, we postannealed both SnO_2 and ZnO nanobelt samples for 1 h in a pure oxygen atmosphere at 900 °C. After the annealing process, Raman data were collected from both nanobelt samples at a 514.5-nm excitation wavelength. The results of these measurements are presented in Figure 4. Dramatic changes in the Raman features can be seen in the figure. The annealed SnO_2 nanobelts now exhibited the spectra corresponding to bulk SnO_2, and the peaks associated with oxygen deficiency in the annealed ZnO nanobelt sample disappeared. Electron and X-ray diffraction studies confirmed that nanobelt structure prevailed in the postannealed samples.
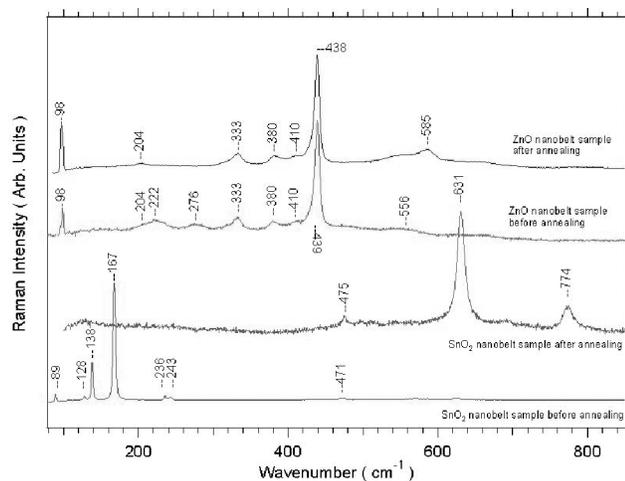
Fig. 4. Comparison of Raman data taken from as-prepared and postannealed nanobelt samples.

4. CONCLUSIONS

No quantum size effects on the phonon structure of nanobelt samples were observed in this study. Room-temperature Raman data of as-prepared nanobelt samples exhibited peaks that corresponded to those expected in oxygen-deficient semiconducting SnO_2 and ZnO. Raman peaks corresponding to bulk SnO_2 and ZnO were observed in nanobelt samples after postannealing in oxygen for 1 h at 900 °C.

References and Notes

1. Zheng Wei Pan, Zu Rong Dai, and Zhong Lin Wang, *Science* 291, 1947 (**2001**).

2. K. L. Chopra, S. Major, and D. K. Pandya, *Thin Solid Films* 102, 1 (**1983**).

3. D. Kohl, *Sens. Actuators*, *B* 1, 158 (**1990**).

4. X. L. Xu, S. P. Lau, J. S. Chen, G. Y. Chen, and B. K. Tay, *J. Cryst. Growth* 223, 201 (**2001**).

5. M. H. Huang, S. Mao, H. Feick, H. Yan, Y. Wu, H. Kind, E. Weber, R. Russo, and P. Yang, *Science* 292, 1897 (**2001**).

6. L. Abello, B. Bochu, A. Gaskov, S. Koudryavtseva, G. Lucazeau, and M. Roumyantseva, *J. Solid State Chem.* 135, 78 (**1998**).

7. P. S. Peercy and B. Morosin, *Phys. Rev. B: Solid State* 7, 2779 (**1973**).

8. R. S. Katiyar, P. Dawson, M. M. Hargreave, and G. R. Wilkinson, *J. Phys. C: Solid State Phys.* 4, 2421 (**1971**).

9. L. Sangaletti, L. E. Depero, B. Allieri, F. Pioselli, E. Comini, G. Sberveglieri, and M. Zocchi, *J. Mater. Res.* 13, 2457 (**1998**).

10. L.-Z. Yang, Z.-T. Sui, and C.-Z. Wang, *J. Solid State Chem.* 113, 221 (**1994**).

11. G. Murken and M. Trömel, *Z. Anorg. Allg. Chem.* 397, 117 (**1973**).

12. J. Geurts, S. Rau, W. Richter, and F. J. Schmitte, *Thin Solid Films* 121, 217 (**1984**).

13. H. Olijnyk, *Phys. Rev. B: Solid State* 46, 6589 (**1992**).

14. PHONON is described online at http://wolf.ifj.edu.pl/phonon/.

15. Z. R. Dai, J. L. Gole, and J. D. Stout, Z. L. Wang, *J. Phys. Chem. B* 106, 1274 (**2001**).

16. C. Xie, L. Zhang, and C. Mo, *Phys. Status Solidi A* 141, K59 (**1994**).

17. J. Zuo, C. Xu, X. Liu, C. Wang, Y. Hu, and Y. Qian, *J. Appl. Phys.* 75, 1835 (**1994**).

18. L. Abello, B. Bochu, A. Gaskov, S. Koudryavtseva, G. Lucazeau, and M. Roumyantseva, *J. Solid State Chem.* 135, 78 (**1998**).

19. K. Parlinski and Y. Kawazoe, *Eur. J. Phys. B* 13, 679 (**2000**).

20. M. Tzolov, N. Tzenov, D. Dimova-Malinovska, C. Pizzuto, G. Vitali, G. Zollo, and I. Ivanov, *Thin Solid Films* 379, 28 (**2000**).

21. G. J. Exarhos, A. Rose, and C. F. Windish, Jr., *Thin Solid Films* 308–309, 56 (**1997**).

22. M. Rajalakshmi and A. K. Arora, *J. Appl. Phys.* 87, 2445 (**2000**).

23. J. M. Calleja and M. Cardona, *Phys. Rev. B: Solid State* 16, 3753 (**1977**).

24. X. L. Xu, S. P. Lau, J. S. Chen, G. Y. Chen, and B. K. Tay, *J. Cryst. Growth* 223, 201 (**2001**).